BUCKLING OPTIMIZATION OF STEERING STIFFENERS FOR GRID-STIFFENED COMPOSITE STRUCTURES

Dan WANG and Mostafa M. ABDALLA
Department of Aerospace Structures and Materials, Delft University of Technology
2629 HS Delft, The Netherlands
Email: d.wang@tudelft.nl, m.m.abdalla@tudelft.nl

Keywords: Curved stiffeners, Optimization, Grid-stiffened composite structures, Global and local buckling

ABSTRACT

Grid-stiffened composite structures, where the skin is stiffened by a lattice of stiffeners, not only allow for significant reduction in structural weight but are also competitive in terms of structural stability and damage tolerance compared with sandwich composite structures. As the development of Automated Fiber Placement (AFP) technology matures, integrated construction of skin and stiffeners is easily manufacturable. Optimization of grid-stiffened structures is needed to fully take advantage of the expanded design possibilities. In this paper, a steering/curved stiffener layout is optimized for grid-stiffened composite structures in order to enhance the structural buckling resistance. A homogenization method is used to calculate the equivalent material properties. Global and local buckling loads are determined by a global/local coupled strategy. A linear variation of stiffener angles is assumed resulting in the formation of a locally rhombic lattice pattern by the stiffeners. Moreover, manufacturing constraints are considered in the optimization by setting a lower bound on the stiffener spacing. Since the calculation is implemented on an equivalent model with a fixed mesh, it is possible to use a gradient-based optimization algorithm. A comparison between the performance of grid-stiffened composite structures with curved stiffeners, with straight stiffeners, and with variable-stiffness skins with curved fibers, reveals the potential of curved stiffener configurations in improving structural efficiency.

1 INTRODUCTION

Grid stiffened aluminum structures have been used in aerospace applications for several decades and still play an important role in space launch vehicles. Driven by exceptional high stiffness, and strength, to weight ratios of Fiber Reinforced Plastic composites (FRPs), early study of grid-stiffened composite structures began in the late 1970s by research groups in the USA and the USSR for space applications [1-2]. However, the development of grid-stiffened composite structures was highly limited by the expensive cost and the precarious quality of the labor intensive manual manufacturing. By the 1990s, automated manufacturing techniques greatly boost the growth of these promising composite structures. Advanced automated robotic fiber placement systems make the manufacturing process practical for complex composite structures. By using these and similar technologies, grid-stiffened composite structures can be manufactured efficiently and cheaply as an integrated structure. Nowadays, they can be up to 30% cheaper to produce than existing sandwich composite structures in addition to their other advantages, such as high damage tolerance, light weight and low moisture expansion [3].

The exceptional performance and affordable manufacturing cost of grid-stiffened composite structures make them the subject of renewed interests from both academia and industry. Grid-stiffened composite structures offer a wide choice in both the skin layup and the stiffener configuration and provide a natural arena for the application of optimization techniques. If this selective tailoring is combined with clever selection of structural layout, exceptionally light and efficient composite structures may be designed. Discrete ply angles of skin laminate, stiffener sizing and stiffener spacing are commonly used as design variables for parametric studies [4] and optimization with a discrete optimizer [5-7]. Improving the computational efficiency is a key for the optimization design for grid-stiffened composite structures since the discrete optimization is implemented based on a large number of sample points. Using analytical [8-9] or equivalent homogeneous models [10-11] can effectively save computational time. But analytical models have limited applicability due to demanding requirements for specific boundary conditions, loading cases and grid patterns, while equivalent models are unable to capture local behavior. A combination of detailed models and the equivalent model is used as hybrid models for local detailed grid-stiffened structures [12].

Besides the above-mentioned design variables, proper tailoring of stiffener directions can provide optimal distribution of stiffness throughout the structure and further improve the structural performances. A curved stiffener distribution is selected to reduce the weight for a potential application on a low loading part of a fuselage barrel [13]. It is shown that optimal varying angle ribs have the ability to improve the axial global buckling capacity of elliptical grid stiffened cylinders [14]. Kapania and his co-authors' work shows that proper placements of curved stiffeners on buckling dominated metallic panels may lead to a reduced structural weight with buckling constraints than that with straight stiffeners [15-16]. In their work, curved stiffener paths are modeled by a third order rational spline on a bounding box [17]. Their research efforts comprise curved stiffener modeling [18-19], global optimization algorithms [20] and an integrated design environment [21].

Other research on the subject of stiffener layout design relates to topology optimization techniques. A layer-wise element [22] or a micro-structure [23-25] is used in topology optimization and may achieve a design with discontinuous or lumped reinforcement regions. These designs negate the exceptional damage tolerance of grid-stiffened structures which is due to the high redundancy of the ribs. Moreover, the jagged boundaries of the design generated by topology optimization makes it difficult to manufacture and a lot of subsequent post-processing work is required. Discrete beam models [26] are also used with similar problems in generating a clear continuous stiffener layout.

Realistic stiffener layout design for composite structures faces the following difficulties: (a) appropriate definition of stiffener paths; (b) multiply highly-coupled failure modes; (c) separation of stiffener paths from mesh generation. An unfortunate choice of design variables for stiffener paths will either cause a large number of design variables or a noneffective design. Absence of some critical failure modes will make the design useless. A mesh-dependent stiffener definition will prevent, or complicate, the application of an efficient gradient-based optimization algorithm.

In this paper, parametric, optimization and post-buckling analysis of flat panels stiffened by a curved stiffener lattice are investigated. In Section 2, curved stiffener paths are defined based on a linear variation of stiffener angles and a global/local coupled strategy for buckling load calculations is presented. In Section 3, results of a parametric design study and optimization for shallow curved stiffener designs are compared and discussed. In Section 4, one set of optimal straight and curved stiffener designs are compared with results of a detailed finite element model, which is further used in post-buckling analysis. Conclusions are given in Section 5.

2 BUCKLING ANALYSIS OF CURVED STIFFENER DESIGNS

2.1 Definition of curved stiffener paths

As illustrated in Fig. 1, a uniaxially compressed square panel with a length of $2a$ and a thickness of t is selected as the baseline design. In the paper, stiffened panels with straight and curved stiffeners are designed with the same volume as the baseline design.

Because of symmetry, a fourth of stiffener paths are designed. Linear variation of stiffener angles is used to generate a reference stiffener path, as expressed in Eq. (1):

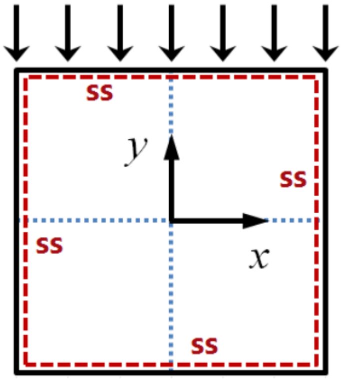

Figure 1: Schematic diagram of the involved panel.

$$\theta = \theta_1 + \frac{\theta_2 - \theta_1}{a} x \tag{1}$$

As illustrated in Fig. 2, stiffener paths are generated by a series of mirroring and shifting operations based on the reference stiffener path. The definition was used to describe curved fibre paths in variable-stiffness skin designs and proven to be effective [27].

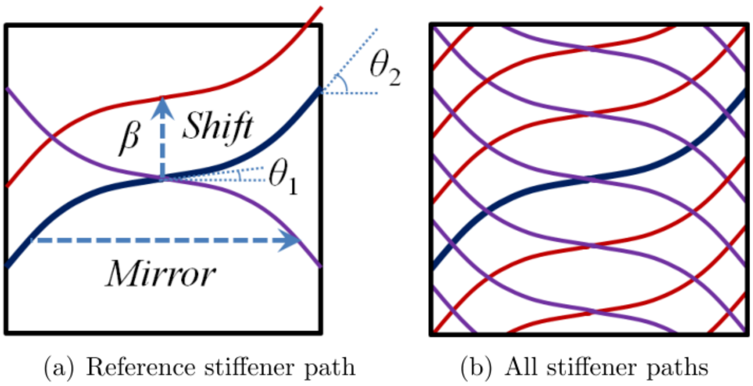

Figure 2: Curved stiffener path generation.

Thus, the stiffener path satisfies the following expression:

$$\frac{\mathrm{d}y}{\mathrm{d}x} = \tan\theta \tag{2}$$

Substituting of Eq. (1) and integrating, the reference stiffener path is formulated as:

$$y = \begin{cases} x\tan\theta_1, & if\ \theta_1 = \theta_2 \\ \dfrac{a}{\theta_1 - \theta_2}\ln\dfrac{\cos\theta}{\cos\theta_1}, & if\ \theta_1 \neq \theta_2 \end{cases} \tag{3}$$

The length of a continuous stiffener with x=(-a, a) can be calculated by the following equation:

$$l = 2\int_0^a \sqrt{\mathrm{d}^2x + \mathrm{d}^2y} = \begin{cases} \dfrac{2a}{\cos\theta_1}, & if\ \theta_1 = \theta_2 \\ \dfrac{2a}{\theta_2 - \theta_1}\ln\left(\dfrac{\sec\theta_2 + \tan\theta_2}{\sec\theta_1 + \tan\theta_1}\right), & if\ \theta_1 \neq \theta_2 \end{cases} \tag{4}$$

Because all the other stiffener paths from the same family are a shift along y direction from the reference path expressed by Eq. (3) and stiffener paths from the other family are a mirror of those from the first family, the total length of stiffener paths is expressed as:

$$l_{all} = \frac{4b}{\beta} l \tag{5}$$

where β is the shift dimension between two neighboring stiffeners along y direction.

2.2 Stiffener volume calculation

Volume of stiffeners is expressed as:

$$V_{stiff} = whl_{all} = \begin{cases} \frac{8abwh}{\cos\theta_1}, & if\ \theta_1 = \theta_2 \\ \frac{8abwh}{\beta(\theta_2 - \theta_1)} \ln\left(\frac{\sec\theta_2 + \tan\theta_2}{\sec\theta_1 + \tan\theta_1}\right), & if\ \theta_1 \neq \theta_2 \end{cases} \tag{6}$$

with w and h denote the stiffener width and height respectively.

As illustrated in Fig. 3, there is additional length due to local stiffener steering in the manufacturing process. The change in length at one intersection node Δl may be approximated as:

$$\frac{\Delta l}{H} = \frac{2}{3}\sqrt{\frac{H}{R}} \tag{8}$$

Assume that H=1 tow width and R=100 tow widths. Then, Δl= 1/15.

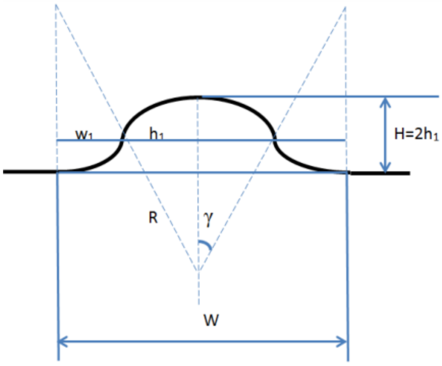

Figure 3: Local steering path around the intersection node.

Therefore, the stiffener volume will be rewritten as:

$$V_{stiff}^{*} = wh(l_{all} + n\Delta l) \tag{7}$$

where n denotes the number intersection nodes and can be formulated as:

$$n = \int_{-b}^{b}\int_{-a}^{a} \rho dxdy = \begin{cases} \frac{8ab\tan\theta_1}{\beta^2}, & if\ \theta_1 = \theta_2 \\ \frac{8ab}{\beta^2(\theta_1 - \theta_2)} \ln\frac{\cos\theta_2}{\cos\theta_1}, & if\ \theta_1 \neq \theta_2 \end{cases} \tag{9}$$

2.3 Buckling load calculations [28]

As illustrated in Fig. 3, a global/local coupled strategy is used to calculate both global and local buckling loads of the curved grid-stiffened composite structures.

The equivalent material properties are calculated based on the asymptotic homogenization method by keeping the strain energy of the equivalent cell the same as that of the stiffened cell. By using the equivalent material properties, the global buckling load can be calculated based on a homogenized panel. With global strains and curvatures of the equivalent model as inputs, the local responses of the stiffened structure can be calculated based on characteristic cells. These local responses on one hand can be used for material failure calculation and on the other hand are inputs for local buckling load calculation. Bloch wave theory, as an alternative to capture the local instability in a periodic medium, presents displacements of a particle as a product of a periodic component with the same periodicity as the medium and a periodic function related to an arbitrary wavelength. It's proved that the onset of instability of periodic solids can be determined by the Bloch wave theory [29]. In the application of grid-stiffened structures, the local minimum of the buckling load surface corresponds to the critical local buckling load. Based on an assembly of the skin and stiffeners in a characteristic cell, the critical local buckling load is captured no matter whether it is skin pocket buckling, stiffener crippling or a coupling of both. The interested reader may consult the details in [28].

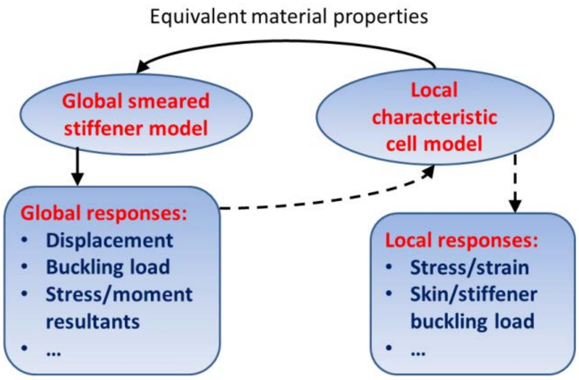

Figure 4: Global/local coupled strategy.

3 PARAMETRIC STUDY AND OPTIMIZATION DESIGN

The baseline panel is made up of 20 plies and the stacking sequence is $[\pm 45]_{5s}$ [27]. The buckling and failure load factors of the baseline panel under a uniform compression are listed in Table 1. The average ply thickness of the baseline panel and the variable-stiffness (VS) panel with overlaps is 0.19432 *mm*, while that of the VS panel without overlaps is 0.18923 *mm*. From the comparison, it is found that the buckling load factor of the baseline panel predicted by the present authors is close to the value in [27] with a 5.14% difference. To make the results conservative and also comparable with the VS panel without overlaps, the smaller average ply thickness of 0.18923 *mm* is used in the following stiffener designs.

Table 1: Buckling and failure load factors for the baseline panel.

	Configuration	λ_g Eigenvalue analysis	λ_g Measured	λ_{fail} Measured
Ref. [28]	$[\pm 45]_{5s}$, t_{ply}=0.19432	38.6738	27.7284	196.2880
	VS panel w/o overlaps	43.7817	67.1320	205.0443
	VS panel w overlaps	84.6446	99.2385	299.9047
Present	$[\pm 45]_{5s}$, t_{ply}=0.19432	36.6846	\	\
	$[\pm 45]_{5s}$, t_{ply}=0.18923	33.8819	\	\

For both straight and curved stiffener designs, the total volume is kept the same as that of the baseline panel. Volume ratios of 2/3, 3/2 and 4 are used between the skin and stiffeners and correspond to skin of 8, 12 and 16 plies, respectively.

3.1 Definition of the design problem

The optimization model is mathematically expressed as:

$$\begin{cases} Find: \quad [\theta_1, \theta_2, \beta] \\ \max: \lambda_g \\ s.t. \\ \qquad p\lambda_g \le \lambda_l \\ \qquad s^L \le s_k, \qquad k = 1, 2 \\ \qquad h \le h^U \end{cases} \tag{10}$$

where λ_g and λ_l are the critical global and local buckling load factors, respectively. p is a penalty factor bigger than one to make sure global buckling dominate the failure mode instead of local buckling in the post-buckling stage. s_k is the stiffener spacing according to θ_k and satisfies $s_k = \beta \cos\theta_k$. Due to the linear variation of stiffener angles, the lower value of these two spacings is the minimum spacing in the design. s^L is the lower bound of the stiffener spacing and depends on the manufacturing requirements. h is the stiffener height and h^U is its upper bound.

Shallow stiffener designs with four times of the skin thickness as the maximum stiffener height are investigated. Firstly, a parametric study is performed in order to investigate the design space. Then, optimal results are provided for comparison. Noticeably, in the parametric study a fixed stiffener height at the upper bound, which means a fixed β, is used while the stiffener height is changeable with an upper bound in optimization. Moreover, to simplify the calculation process, the small additional weight at the stiffener intersections is not included in the parametric study.

3.2 Parametric analysis

The variation with respect to the two design angles of θ_1 and θ_2 is illustrated in Figs. 5-7 for a skin of 8, 12 and 16 plies, respectively. The corresponding skin layups are $[\pm 45]_{ns}$ with n=2,3,4.

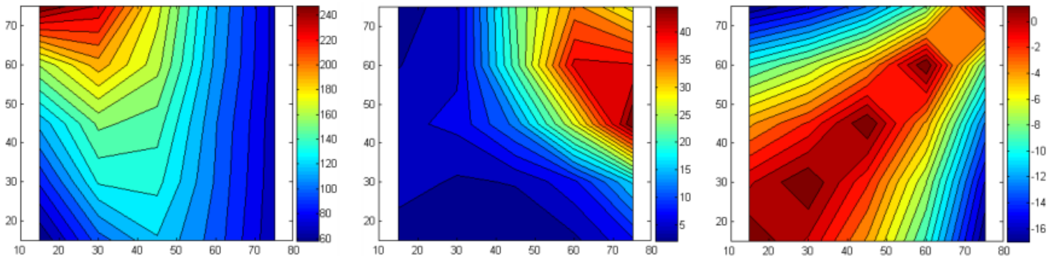

(a) λ_g (b) $\lambda_l/(1.5\lambda_g)$ (c) $s_k - s^L$

Figure 5: Parametric results for a 8 plies skin with h=4t_{skin}.

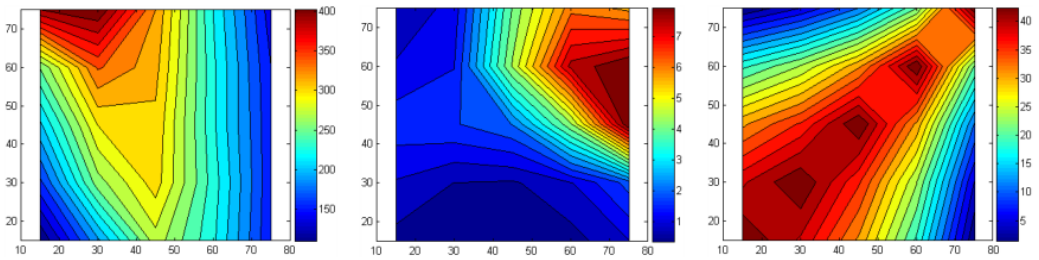

(a) λ_g (b) $\lambda_l/(1.5\lambda_g)$ (c) $s_k - s^L$

Figure 6: Parametric results for a 12 plies skin with h=4t_{skin}.

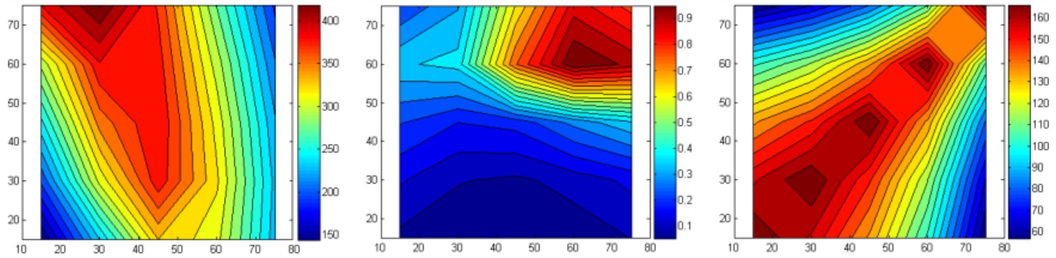

(a) λ_g (b) $\lambda_l/(1.5\lambda_g)$ (c) $s_k - s^L$

Figure 7: Parametric results for a 16 plies skin with h=4t_{skin}.

It is clearly seen that the maximum global buckling load is obtained around the point of θ_1=15~30^o and θ_2=75^o for three different cases if both the local buckling load constraint and the minimum spacing constraint are not considered. It accords with the optimal results for curved fiber skin design [27]. From Fig. 5, it is shown that for relatively thin skin design the minimum stiffener spacing constraint is violated when two design angles are a little different, while for most sampled points the local buckling load has a large safety margin. So the design space is narrowed down and the optimal is located around the point of θ_1=θ_2=45^o. For a 12 plies skin design, the minimum spacing constraint is always inactive and the optimal is located around the point of θ_1=30^o and θ_2=75^o with an active local buckling load constraint. As for a 16 plies skin design, the limited volume for stiffeners causes an invalid design space with no sufficient local buckling load, which means a three-dimensional design with a changeable stiffener height is required.

It is concluded that, with the skin volume fraction increases, the active constraint switches from the minimum spacing to local buckling load. At the same time, the optimal configuration and the effect of stiffener steering will highly depend on the specific configuration.

3.3 Optimization

Optimization results are illustrated in Table 2. When θ_1=θ_2 in the design, optimal straight stiffener distributions are obtained. The optimal configurations agree with the results in the parametric analysis. From the comparison, it is concluded that stiffener steering has a remarkable influence on the global buckling load increase for grid-stiffened composite panels. However, with an enhanced skin stiffness along the compressed direction, an quasi-isotropic skin of [0, ±30, ±60, 90]$_s$ will largely reduce the effect of stiffener steering, as shown in Table 3. For a 16 plies skin, the improvement by stiffener steering for a quasi-isotropic layup is a little larger than [±45]$_{4s}$ due to the advantage of a changeable stiffener height.

Table 2: Optimization results for shallow stiffener design with a skin layup of [±45]$_{ns}$.

Skin plies	Stiffeners	Design variables			λ_g	Constraints			Buckling increase
		$\theta_1(^o)$	$\theta_2(^o)$	$\beta(mm)$		$\frac{\lambda_l}{\lambda_g}$	$\frac{s_{\min}}{s^L}$	$\frac{h}{t_{skin}}$	
8	Curved	39.84	48.53	47.94	156.96	15.38	1.00	4.00	4.31%
	Straight	39.13	\	44.19	150.47	7.88	1.08	4.00	\
12	Curved	27.64	77.97	152.34	431.36	1.50	1.00	4.00	35.27%
	Straight	39.71	\	99.59	318.88	1.50	2.41	4.00	\
16	Curved	46.75	59.25	304.80	313.86	1.50	4.91	3.57	20.78%
	Straight	55.12	\	303.02	259.86	1.50	5.46	3.40	\

The optimal configurations for a 12 plies skin with a layup of [± 45,0, ±45, 90]$_s$ and a 16 plies skin with a layup of [±45, 0, 90]$_{2s}$ are given in Fig. 8.

Table 3: Optimization results for shallow stiffener design with a quasi-isotropic skin layup.

Skin		Stiffeners	Design variables			λ_g	Constraints			Buckling
Plies	Layup		$\theta_1(^o)$	$\theta_2(^o)$	$\beta(mm)$		$\frac{\lambda_l}{\lambda_g}$	$\frac{s_{\min}}{s^L}$	$\frac{h}{t_{skin}}$	increase
12	$[\pm45, 0, \pm45, 90]_s$	Curved	20.31	76.85	139.53	368.75	1.66	1.00	4.00	15.15%
		Straight	38.37	\	97.72	320.21	1.50	2.41	4.00	\
	$[0, \pm30, \pm60, 90]_s$	Curved	18.20	76.54	136.40	350.39	2.56	1.00	4.00	10.77%
		Straight	36.71	\	95.56	316.32	1.66	2.41	4.00	\
16	$[\pm45, 0, 90]_{2s}$	Curved	46.34	62.85	304.80	293.54	1.50	4.38	3.41	27.71%
		Straight	58.35	\	304.80	229.84	1.50	5.03	3.14	\

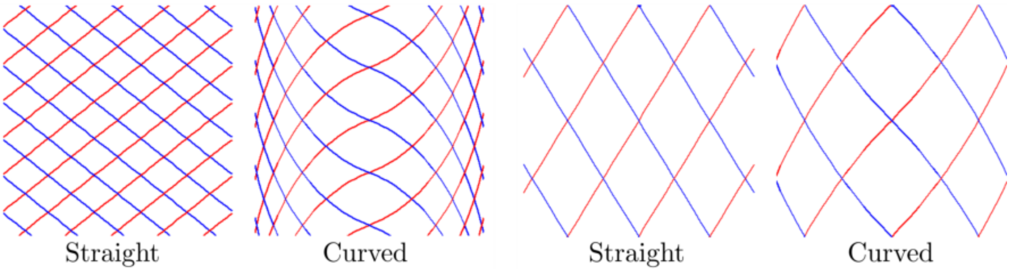

(a) A 12 plies skin of $[\pm45, 0, \pm45, 90]_s$ (b) A 16 plies skin of $[\pm45, 0, 90]_{2s}$

Figure 8: Optimal configurations for shallow stiffener design.

4 POST-BUCKLING ANALYSIS

From Table 3 and Fig. 8, it seems that slightly curved stiffeners in a quasi-isotropic skin with 16 plies will cause an improvement of 27.71% in global buckling load, and the sparse stiffener distribution and shallow stiffener height will be easily manufacturable and will be a good option as an enhanced ski for a larger stiffened structure. Therefore, this candidate is selected to do post-buckling calculation.

Global and local buckling modes of the detailed model with rounded-off parameters of the straight stiffener design of θ_1=θ_2=59^o and the curved stiffener design of θ_1=45^o and θ_2=65^o are illustrated in Fig. 9. We indicate the predicted global buckling load of the detailed model, which may be considered the limit load, and the corresponding ultimate load (1.5 times). It is clear that very significant post buckling strength remains.

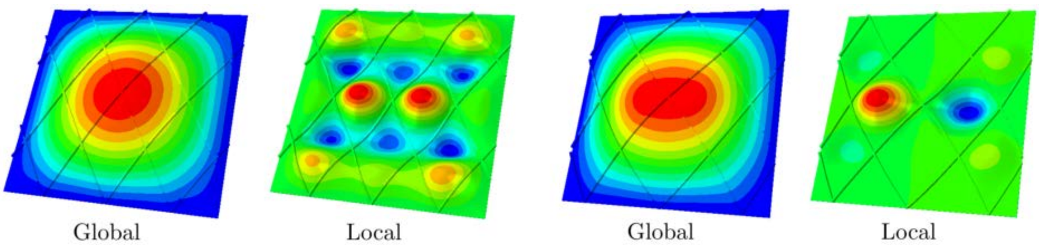

(a) Straight stiffeners (b) Curved stiffeners

Figure 9: Global and local buckling modes of the detailed model with a skin of $[\pm45, 0, 90]_{2s}$.

The comparison between optimal results of detailed model and equivalent model with a skin of $[\pm45, 0, 90]_{2s}$ are given in Table 4. The sparsely distributed stiffeners make the global local modeling less accurate than for denser grid configurations. Therefore both global and local buckling load predictions in the equivalent model have a relatively large error compared with the detailed model. However, since the global buckling load factors for both cases are overestimated by roughly the same amount, the improvement due to the stiffener steering still remains to be about 30%.

Table 4: Comparison between optimal results of detailed model and equivalent model with a skin of [±45, 0, 90]$_{2s}$.

	Straight			Curved			Buckling increase
	λ_g	λ_l	λ_l/λ_g	λ_g	λ_l	λ_l/λ_g	
Detailed model	158.36	592.27	3.74	206.17	437.08	2.12	30.19%
Equivalent model	220.89	362.26	1.64	285.78	505.83	1.77	27.71%
Error	39.48%	-38.99%	\	38.60%	15.46%	\	\

Load factor vs end-shortening curves for both straight and curved stiffener designs are illustrated in Fig. 10.

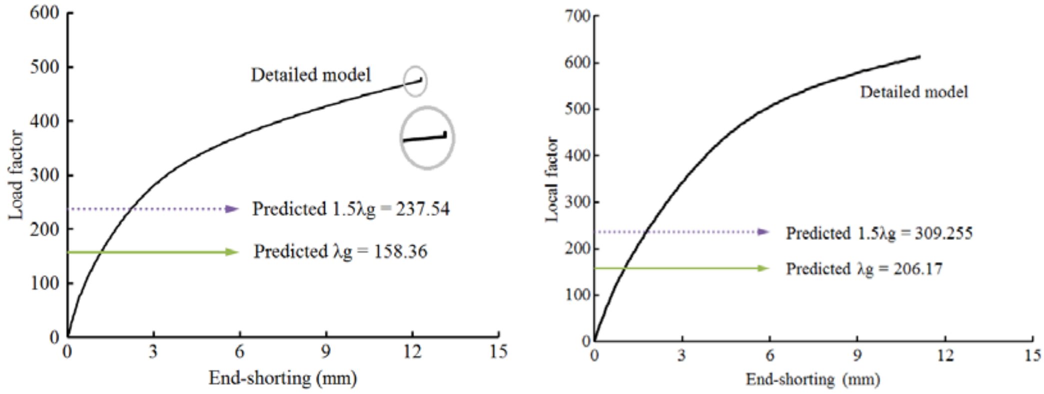

(a) Straight stiffener design (b) Curved stiffener design

Figure 10: Load factor vs end-shortening curves.

Out-of-plane displacements are illustrated in Fig.s 11 and 12. Similarly in two cases, in the post-buckling stage, global buckling dominates the deformation shape. At the maximum loading in the nonlinear calculation, local deformations emerge, which might indicate the interaction between global and local buckling modes and accords with the singularity at the end of the load factor vs end-shortening curves.

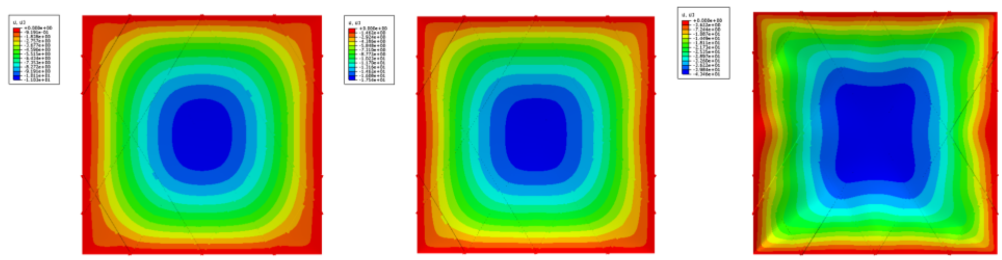

(a) Limit load: 158.36 $\min(U_3) = -11.03mm$ (b) Ultimate load: 237.54 $\min(U_3) = -17.54mm$ (c) Maximum load: 479.721 $\min(U_3) = -43.46mm$

Figure 11: Out-of-plane displacements of the straight stiffener design with a skin of 16 plies.

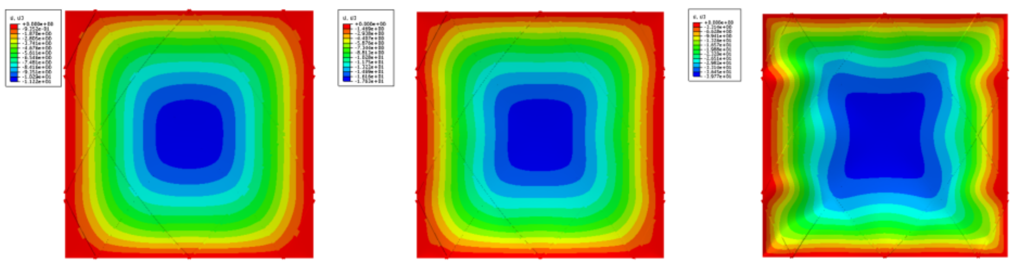

(a) Limit load: 206.17 $\min(U_3) = -11.22mm$ (b) Ultimate load: 309.255 $\min(U_3) = -17.63mm$ (c) Maximum load: 611.962 $\min(U_3) = -39.77mm$

Figure 12: Out-of-plane displacements of the curved stiffener design with a skin of 16 plies.

The distribution of the stress resultants along the compressed direction of the straight and curved stiffener designs are illustrated in Fig.s 13 and 14, respectively. According to these figures, it is found that the middle part of the panel is even under tension due to the bending induced by lack of out of plane symmetry. In the curved stiffener design, stiffeners are more densely distributed at the two sides, from which the superiority of curved stiffener design is shown in the post-buckling region.

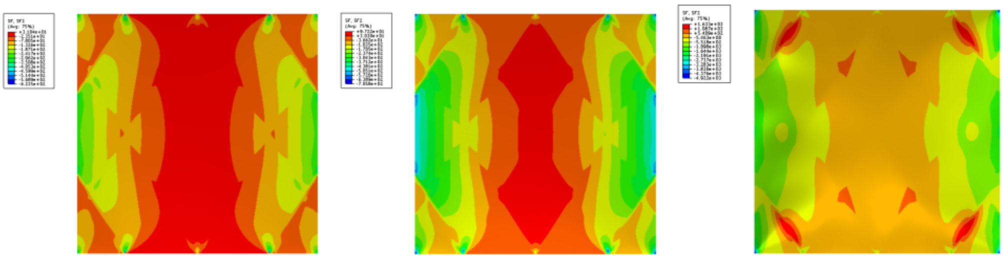

(a) Limit load: 158.36 $\max(S_2) = 31.04$ $\min(S_2) = -623.5$

(b) Ultimate load: 237.54 $\max(S_2) = 97.22$ $\min(S_2) = -705.8$

(c) Maximum load: 479.721 $\max(S_2) = 1633$ $\min(S_2) = -4922$

Figure 13: Stress resultants along the compressed direction of the straight stiffener design with a skin of 16 plies.

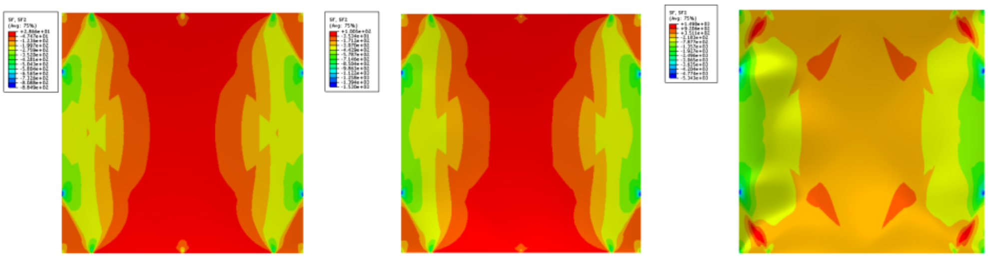

(a) Limit load: 158.36 $\max(S_2) = 28.66$ $\min(S_2) = -884.9$

(b) Ultimate load: 237.54 $\max(S_2) = 100.5$ $\min(S_2) = -1530$

(c) Maximum load: 479.721 $\max(S_2) = 1490$ $\min(S_2) = -5343$

Figure 14: Stress resultants along the compressed direction of the curved stiffener design with a skin of 16 plies.

The remarkably increased buckling load by adding stiffeners will largely increase the risk of material failure due to large strains. To investigate this phenomenon, in-plane principal strain distributions at both the limit loading and ultimate loading are given in Table 4. The strain concentrations at four corners due to the boundary conditions are not considered. From the strain distributions, it is found that the maximum strains are located at the interfaces between the skin and stiffeners close to the compressed boundaries, which on one hand means the strain concentration might be slightly released in practice by proper introduction of loads and on the other hand indicates that material failure might be critical. The curved stiffener design has a higher risk compared to the straight stiffener design.

5 CONCLUSIONS

Curved stiffener layouts for stiffening composite skins are investigated in the paper. The layout is based on linearly varying stiffener angles. Compared with the variable-stiffness skin designs, even shallow straight stiffeners will lead to a remarkable increase in the buckling load for the same structural volume. The buckling value of the stiffened panel is even comparable with the measured failure load of a variable-stiffness panel. This superiority is maintained in the post-buckling stage by enforcing the local buckling load higher than the global buckling load with a safety factor in design optimization. Curved stiffeners further improve the structural stability by redistributing the load. In optimal configurations with curved stiffeners, the stiffeners are densely distributed at the boundaries, which reduces the central loading by distributing more load at the boundaries. The difference in stiffener angles for an optimal design depends on the specific design problem. Compared with the detailed FE model, predictions of both global and local buckling loads by the equivalent model have a large error for a sparsely stiffened structure. The relative load carrying capacity is well calculated though making the method suitable for the preliminary selection of stiffener layout.

Table 4: Strain distributions for straight and curved stiffener designs with a skin of 16 plies.

Loading		Straight stiffeners	Curved stiffeners
	Load factor	158.36	206.17
Limit	Strains	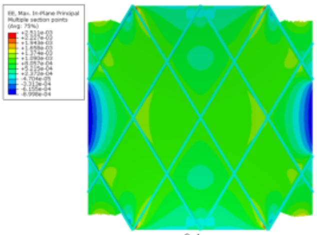	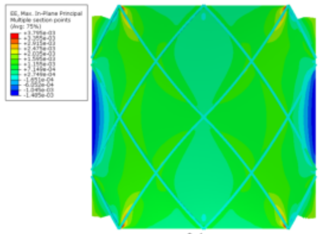
	Maximum	0.2511%	0.3795%
	Load factor	237.54	309.255
Ultimate	Strains	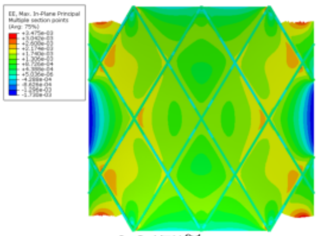	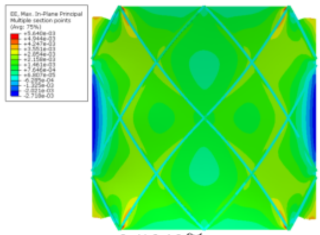
	Maximum	0.3475%	0.5640%

REFERENCES

[1] S. Huybrechts, T. E. Meink, Advanced grid stiffened structures for the next generation of launch vehicles, In *Aerospace Conference, 1997. Proceedings*., IEEE, Vol. 1, IEEE, 1997, pp. 263-270.

[2] S. M. Huybrechts, S. E. Hahn, T. E. Meink, Grid stiffened structures: a survey of fabrication, analysis and design methods, in: T. Massard, A. Vautrin (Eds.), *Proceedings of the 12th International Conference on Composite Materials* (ICCM/12), Paris, France, 1999, pp. 1-10.

[3] C. Collier, P. Yarrington, B. Van West, Composite, grid-stiffened panel design for post buckling using hypersizer, *43rd AIAA/ASME/ASCE/AHS/ASC Structures, Structural Dynamics, and Materials Conference*, Denver, Colorado, 2002, pp. 1-16.

[4] E. Wodesenbet, S. Kidane, S. S. Pang, Optimization for buckling loads of grid stiffened composite panels, *Composite Structures* 60 (2) (2003) 159-169.

[5] N. Jaunky, N. F. Knight, D. R. Ambur, Optimal design of general stiffened composite circular cylinders for global buckling with strength constraints, *Composite structures* 41 (3) (1998) 243-252.

[6] J. Phillips, Z. Gürdal, Analysis and optimal design of geodesically stiffened composite panels, in: *Proceedings of the 2nd Int. Conf. on Computer Aided Design in ComM posite Material Technology*. Free University of Brussels/Wessex Institute of Technology, Computational Mechanics Publications, Southampton, 509M520, 1990.

[7] P. Hao, B. Wang, G. Li, Surrogate-based optimum design for stiffened shells with adaptive sampling, *AIAA journal* 50 (11) (2012) 2389-2407.

[8] S. Shroff, Design, analysis, fabrication and testing of grid-stiffened for fuselage applications, Ph.D. thesis, TU Delft, Delft University of Technology (2014).

[9] L. Friedrich, H. G. Reimerdes, K. U. Schröder, Advanced sizing strategies for preliminary design of orthotropic grid stiffened shell structures, *3rd International Conference on Buckling and Postbuckling Behaviour of Composite Laminated Shell Structures with DESICOS Workshop*, 2015.

[10] J. Kato, D. Yachi, K. Terada, T. Kyoya, Topology optimization of micro-structure for composites applying a decoupling multi-scale analysis, *Structural and Multidisciplinary Optimization* 49 (4) (2014) 595-608.

[11] L. Xia, P. Breitkopf, Multiscale structural topology optimization with an approximate constitutive model for local material microstructure, *Computer Methods in Applied Mechanics and Engineering* 286 (2015) 147-167.

[12] H. J. Chen, S. W. Tsai, Analysis and optimum design of composite grid structures, *Journal of composite materials* 30 (4) (1996) 503-534.

[13] W. van den Brink, W. Vankan, Design for manufacturing of fuselage panels with curved grid stiffening, Tech. Rep. NLR-TP-2013-310, National Aerospace Laboratory NLR (2013).

[14] M. Paschero, M. W. Hyer, Improvement of axial buckling capacity of elliptical lattice cylinders, *AIAA journal* 49 (2) (2011) 396-410.

[15] R. K. Kapania, J. Li, H. Kapoor, Optimal design of unitized panels with curvilinear stiffeners, *5th ATIO and the AIAA 16th Lighter-than-Air Systems Technology Conference and Balloon Systems Conference*, Vol. 3, 2005, pp. 1708-1737.

[16] M. Bhatia, R. K. Kapania, Stiffener effectiveness approach for optimal stiffener placement on curvilinear stiffened panel, *50th AIAA/ASME/ASCE/AHS/ASC Structures, Structural Dynamics, and Materials Conference 17th AIAA/ASME/AHS Adaptive Structures Conference 11th AIAA*, 2009.

[17] S. B. Mulani, D. Locatelli, R. K. Kapania, Grid-stiffened panel optimization using curvilinear stiffeners, *AIAA paper* (2011-1895) 2011.

[18] A. Y. Tamijani, R. K. Kapania, Buckling and vibration of curvilinearly stiffened plate subjected to in-plane loads using Chebyshev Ritz method, *51st AIAA/ASME/ASCE/AHS/ASC Structures, Structural Dynamics, and Materials Conference*, 2010.

[19] A. Y. Tamijani, R. K. Kapania, Buckling and static analysis of curvilinearly stiffened plates using mesh-free method, *AIAA journal* 48 (12) (2010) 2739{2751.

[20] P. Joshi, S. B. Mulani, R. K. Kapania, Y. Shin, Optimal design of unitized structures with curvilinear stiffeners using response surface methodology, *49th AIAA/ASME/ASCE/AHS/ASC Structures, Structural Dynamics, and Materials Conference*, no. 2008-2304, 2008.

[21] W. C. H. Slemp, R. K. Bird, R. K. Kapania, D. Havens, A. Norris, R. Olli e, Design, optimization, and evaluation of integrally stiffened al-7050 panel with curved stiffeners, *Journal of Aircraft* 48 (4) (2011) 1163-1175.

[22] T. Gao, W. H. Zhang, P. Duysinx, Simultaneous design of structural layout and discrete fiber orientation using bi-value coding parameterization and volume constraint, *Structural and Multidisciplinary Optimization* 48 (6) (2013) 1075-1088.

[23] R. Ansola, J. Canales, J. Tarrago, J. Rasmussen, Combined shape and reinforcement layout optimization of shell structures, *Structural and Multidisciplinary Optimization* 27 (4) (2004) 219-227.

[24] L. A. Krog, N. Olhoff, Optimum topology and reinforcement design of disk and plate structures with multiple stiffness and eigenfrequency objectives, *Computers & Structures* 72 (4) (1999) 535-563.

[25] J. Luo, H. Gea, A systematic topology optimization approach for optimal stiffener design, *Structural optimization* 16 (4) (1998) 280-288.

[26] X. Ding, K. Yamazaki, Stiffener layout design for plate structures by growing and branching tree model (application to vibration-proof design), *Structural and Multidisciplinary Optimization* 26 (1-2) (2004) 99-110.

[27] K. C. Wu, Z. Gürdal, J. H. Starnes, Structural response of compression loaded, tow-placed, variable stiffness panels, *Proceedings of the 43rd AIAA/ASME/ASCE/AHS/ASC structures, structural dynamics and materials conference*, Denver, Co, 2002, pp. 2002-1512.

[28] D. Wang, M. Abdalla, Global and local buckling analysis of grid-stiffened composite panels, *Composite Structures* 119 (2015) 767-776.

[29] G. Geymonat, S. Müller, N. Triantafyllidis, Homogenization of nonlinearly elastic materials, microscopic bifurcation and macroscopic loss of rank-one convexity, *Archive for Rational Mechanics and Analysis* 122 (3) (1993) 231-290.